

Vesicular Glutamate Transport at a Central Synapse Limits the Acuity of Visual Perception in Zebrafish

Matthew C. Smear,^{1,4} Huizhong W. Tao,^{2,3,4} Wendy Staub,¹ Michael B. Orger,¹ Nathan J. Gosse,¹ Yan Liu,² Koji Takahashi,¹ Mu-ming Poo,³ and Herwig Baier^{1,*}

¹University of California, San Francisco, Department of Physiology, Program in Neuroscience, 1550 4th Street, San Francisco, CA 94143, USA

²Zilkha Neurogenetic Institute and Department of Ophthalmology, Keck School of Medicine, University of Southern California, Los Angeles, CA 90033, USA

³Division of Neurobiology, Department of Molecular and Cell Biology, and Helen Wills Neuroscience Institute, University of California, Berkeley, Berkeley, CA 94720, USA

⁴These authors contributed equally to this work.

*Correspondence: herwig.baier@ucsf.edu

DOI 10.1016/j.neuron.2006.12.013

SUMMARY

The neural circuitry that constrains visual acuity in the CNS has not been experimentally identified. We show here that zebrafish *blumenkohl* (*blu*) mutants are impaired in resolving rapid movements and fine spatial detail. The *blu* gene encodes a vesicular glutamate transporter expressed by retinal ganglion cells. Mutant retinotectal synapses release less glutamate, per vesicle and per terminal, and fatigue more quickly than wild-type in response to high-frequency stimulation. In addition, mutant axons arborize more extensively, thus increasing the number of synaptic terminals and effectively normalizing the combined input to postsynaptic cells in the tectum. This presumably homeostatic response results in larger receptive fields of tectal cells and a degradation of the retinotopic map. As predicted, mutants have a selective deficit in the capture of small prey objects, a behavior dependent on the tectum. Our studies successfully link the disruption of a synaptic protein to complex changes in neural circuitry and behavior.

INTRODUCTION

The visual system encodes with high precision the spatio-temporal distribution of photons entering the retina and converts this information into stimulus features, such as motion and contrast. The spacings of photoreceptors, at least in the fovea (Geisler, 1984; Williams and Coletta, 1987), and of retinal ganglion cells (RGCs) (Banks et al., 1991; Wässle and Boycott, 1991) limit how densely images can be sampled by the retina. Phototransduction

kinetics, on the other hand, set an upper bound on the ability to discriminate events in time (Baylor, 1996). In principle, similar considerations apply to the visual circuitry beyond the retina. The spatial resolution of vision must depend on the size and structure of the visual neurons' receptive fields (RFs), which in turn are determined by the arrangement of their synaptic inputs (Barlow, 1975; Reid and Alonso, 1995). Moreover, the kinetics of synaptic transmission from RGCs to visual brain areas should impose limits on the rates at which changes in the visual image are faithfully transmitted (Fortune and Rose, 2001; Tsodyks and Markram, 1997). The neural substrates constraining visual acuity in the CNS, however, have not been identified.

We have taken a combined genetic, electrophysiological, and behavioral approach in zebrafish to this problem. Zebrafish depend on vision for numerous behaviors, including prey capture, predator avoidance, schooling, and reflexes to motion and ambient light (Neuhauss, 2003). Zebrafish RGCs extend axons primarily to the optic tectum, where they each elaborate a single terminal arbor. Each axonal arbor covers about 5%–10% of the tectal surface in the zebrafish larva and may overlap substantially with neighboring arbors (Gnuegge et al., 2001; Schmidt et al., 2000; Stuermer, 1988). The retinotectal projection is highly ordered; neighboring RGCs project to neighboring positions in the tectum, forming a precise retinotopic map (Stuermer, 1988). We investigated the link between retinotopic precision and visual acuity by using the zebrafish *blumenkohl* (*blu*) mutant. Unlike the majority of visual-system mutants discovered in zebrafish (Baier et al., 1996; Muto et al., 2005; Neuhauss et al., 1999), homozygous *blu* mutants are adult viable, show normal electroretinograms, and have normal external morphology.

We first establish that *blu* mutants have difficulty resolving rapidly changing visual scenes, as revealed by their decreased optomotor response (OMR) to the motion of high-temporal frequency gratings (Orger et al., 2000). In

addition, the mutants' spatial acuity is also diminished, as shown both with the OMR assay and with a new behavioral test for prey capture. By positional cloning, we demonstrate that the *blu* mutation disrupts *vglut2a*, encoding a vesicular glutamate transporter closely related to mammalian VGLUT2. This family of proteins mediates glutamate uptake by synaptic vesicles and is necessary for glutamatergic transmission (Bellocchio et al., 2000; Freneau et al., 2001, 2004; Takamori et al., 2001; Wojcik et al., 2004). Zebrafish *vglut2a* is expressed in RGCs and is partially responsible for glutamatergic transmission at the retinotectal synapse. Electrophysiological analysis showed that RGCs in *blu* mutants have two separable phenotypes that compromise the spatial and temporal resolution of vision, respectively. First, retinotectal synapses in mutants exhibit pronounced fatigue during high-frequency stimulation. Second, individual RGC axon arbors cover a larger area in the tectum, leading to an expansion of tectal RFs. Thus, perturbations of neural circuitry, caused by mutation of *vglut2a*, lead to specific perceptual deficits.

RESULTS

The *blu* Mutation Reduces Both Temporal and Spatial Visual Acuity

We previously reported that *blu* mutants showed reduced behavioral responses to moving gratings in the OMR paradigm (Neuhauss et al., 1999). To identify the precise nature of this deficit, we reinvestigated their behavior using a refined, quantitative assay (Orger et al., 2000). In order to be able to rule out nonvisual deficits, such as problems with locomotor coordination, swimming speed, or motivation, we used a motion-nulling technique borrowed from human psychophysics (Chichilnisky et al., 1993; Orger and Baier, 2005). In this variation of the original OMR assay, the stimulus consists of two superimposed components, a reference grating moving in one direction and a test grating moving in the opposite direction (Figure 1A). The fish swim in the direction of the perceptually more salient motion stimulus. The reference grating is constant, and its contrast is chosen to be of some intermediate strength. The test grating, however, varies in contrast and temporal frequency. For a given temporal frequency, at low contrast of the test grating, the fish swim in the direction of the reference grating (left value in Figure 1A), while at high test-grating contrast the fish follow the test stimulus (right value in Figure 1A). At some intermediate contrast, the fish show no net movement (middle value in Figure 1A). This "null contrast" gives an index of sensitivity to that temporal frequency. Because the fish make no net movement at the null contrast, any potential nonvisual deficit does not contaminate the measurement.

We determined the null contrasts for a range of test stimuli of varying temporal frequencies, while holding spatial frequency constant. Sensitivity was defined as the inverse of the null contrast. We discovered that mutants showed normal sensitivity to low temporal frequency

stimuli; i.e., the contrast of the test grating needed to cancel motion of the reference grating was very similar between mutant and wild-type. However, *blu* mutants were impaired at temporal frequencies greater than 2.5 Hz (Figure 1B). Here the null contrasts were significantly higher for mutants than for wild-type. We conclude that *blu* mutants are less able to resolve high temporal frequency motion.

We next tested spatial acuity, again using our motion-nulling method, while holding temporal frequency constant. We found that mutants responded normally to the low spatial frequency gratings but were deficient at high spatial frequencies (Figure 1C). Importantly, the deficits in temporal and spatial resolution appear to be independent of another. For stimuli at a given constant velocity (where spatial and temporal frequency vary together), mutants showed normal sensitivity to low spatial and low temporal frequency stimuli but were substantially less sensitive to stimuli of high spatial and high temporal frequency (Figure 1D). The difference in sensitivity between mutant and wild-type was more pronounced at high velocities than when either temporal or spatial frequencies were increased alone. This suggested to us that the two deficits were additive. Thus, the *blu* mutation impairs two independent functions of visual perception, one important for detecting fast changes in time, the other for resolving fine spatial details.

The *blu* Gene Encodes *Vglut2a* and Is Expressed by Retinal Ganglion Cells

To understand how a single-gene mutation could lead to such a visual processing defect, we decided to positionally clone the *blu* gene. Using microsatellite markers (Shimoda et al., 1999), the *blu*^{tz257} mutation was genetically mapped to a narrow region on chromosome 7 of the zebrafish genome. Linkage analysis yielded a marker, z28221, for which no recombinants were found in 2410 meioses. Sequencing of the genomic region surrounding this marker showed that the marker was contained in the first intron of *vglut2a*, a gene homologous to mammalian vesicular glutamate transporter 2 (Freneau et al., 2001; Takamori et al., 2001). Comparison of full-length mutant and wild-type sequences of *vglut2a* cDNA revealed a 114 bp stretch of sequence absent from the *blu*^{tz257} allele (Figure 2A). This sequence corresponded to the fourth exon of the gene. We found, after sequencing the genome surrounding this exon, that the *blu* allele has a T to A substitution in the conserved consensus sequence GT at the 5' end of the adjacent intron (Figure 2B). This mutation abolishes splicing and thus accounts for the skipped exon (Figure 2C). Loss of the fourth exon creates an in-frame stop codon in the next upstream codon, truncating the protein from 584 to 154 aa and deleting several transmembrane domains. We rescued the mutant phenotype by injection of a phage artificial chromosome (PAC) clone containing the *blu* genomic region into embryos at the one-cell stage. Thirteen of 197 injected fish (and 0 of >200 uninjected fish) scored as wild-type by their pigmentation phenotype were

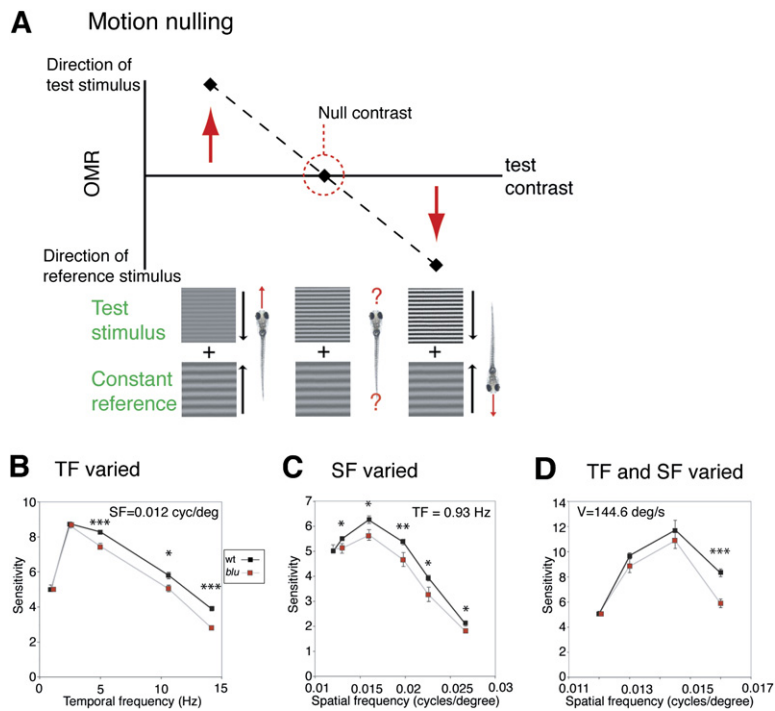


Figure 1. The OMR of *blu* Mutants Shows Reduced Spatial and Temporal Resolution

(A) Schematic diagram of the motion-nulling technique. Stimuli consist of two superimposed drifting sinusoidal gratings, a reference stimulus, held constant across all stimuli, and a test stimulus of a given spatial frequency (SF) or temporal frequency (TF). The test and reference gratings move in opposite directions. For each test stimulus, the contrast is varied. The fish swim in the direction of the more salient motion stimulus, either the reference stimulus (red upward arrow; left point) or the test stimulus (downward arrow; right point). At the null contrast, the reference and test stimuli are of equal strength, and the fish show no net motion (middle point; circled).

(B–D) Visual sensitivity of wild-type and mutants to varying test gratings. The inverse of the “null contrasts” (ranging from 0 to 1) was used as the index of sensitivity to that stimulus. Because the responses of hundreds of fish larvae were averaged, error bars (SEM) are often smaller than the size of the symbols in these graphs. (B) Sensitivity to stimuli of constant SF (0.012 cycles/°) and varying TF. Mutants are less sensitive to high TFs. (C) Sensitivity to stimuli of constant TF (0.93 Hz) and varying SF. Mutants are significantly less sensitive to high SFs. (D) Sensitivity to stimuli of constant velocity ($V = 144.6^\circ/\text{s}$) and increasing SF. TF covaries with SF, according to $V = \text{TF}/\text{SF}$. Mutants are less sensitive to high SFs and TFs. Statistical significance was determined with a two-tailed t test. * $p < 0.05$, ** $p < 0.01$, *** $p < 0.001$.

homozygous *blu* mutants. Taken together, linkage analysis, sequencing, and rescue data show that *blu*^{tz257} encodes a mutant allele of *vglut2a*.

We performed RNA in situ hybridization on whole-mount larvae, as well as isolated larval eyes, at 4 days postfertilization (4 dpf) using antisense oligonucleotide probes. In the wild-type retina, *vglut2a* (*blu*) is prominently expressed in all RGCs, but not in glutamatergic cell types presynaptic to RGCs, such as photoreceptors and bipolar cells (Figures 3A and 3B). The *vglut2a* gene is also expressed in other parts of the brain, including the olfactory system, the pineal, and the ventral diencephalon. In *blu* mutants, we did not detect significant levels of *vglut2a* transcript in the brain or in the eye (Figures 3C and 3D). The absence of mutant RNA is probably due to nonsense-mediated decay. We investigated two other zebrafish *vglut* isoforms (*vglut1a* and *vglut2b*) (Higashijima et al., 2004). The *vglut1a* transcript is expressed in bipolar cells and, more weakly, in RGCs (Figures 3E and 3F). No change in *vglut1a* expression level was detectable in *blu* mutants (data not shown). The *vglut2b* transcript was prominently expressed in distinct brain areas, in a pattern similar to *vglut2a*, but was not detected in the eye of either wild-type or mutant (Figures 3G and 3H). The sense controls of any of these probes showed no signal (data not shown). Our localization studies allow us to conclude (1)

that *vglut2a* is expressed by wild-type RGCs, but not by neurons presynaptic to them; (2) that *vglut1a* is expressed by RGCs and bipolar cells in the retina; (3) that *vglut2a* RNA is completely absent in *blu* mutants, likely rendering retinotectal synaptic transmission dependent on *vglut1a*; and (4) that *vglut1a* and *vglut2b* levels are not upregulated, or otherwise altered, in *blu/vglut2a* mutants. The rather mild phenotype of our *blu* mutant is best explained by redundancy of *vglut* family members at most glutamatergic synapses in the zebrafish brain.

Vglut2a Mutants Show Impairments in the Presynaptic Release of Glutamate

Vesicular glutamate transporters are necessary (Frémeau et al., 2004) and sufficient (Takamori et al., 2001) for glutamatergic neurotransmission. To test the effect of the *blu* mutation on glutamate release by RGC axon terminals, we recorded from postsynaptic neurons in the optic tectum in vivo using whole-cell patch recordings, similar to recordings in *Xenopus laevis* (Engert et al., 2002; Zhang et al., 1998). Tectal neurons in mutants are not different from wild-type in their basic electrophysiological properties (resting membrane potential and input resistance: mutant, 53 ± 6 mV, 1535 ± 128 M Ω , $n = 25$; wild-type, 54 ± 5 mV, 1498 ± 115 M Ω , $n = 22$). Synaptic responses elicited by electrically stimulating the RGC inputs are

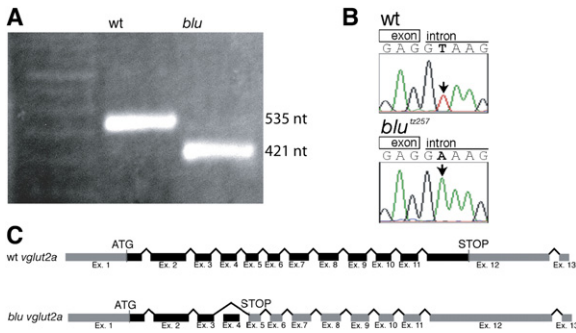


Figure 2. The *blu* Gene Encodes Vglut2a

(A) RT-PCR amplification of a fragment of *vglut2a* containing exon 4. Subsequent sequencing showed that the wt fragment is 535 nt, and the *blu* fragment is 421 nt.

(B) Genomic DNA sequence from the 5' splice site affected in *blu*^{tz257}.

(C) Schematic representation of the *vglut2a* gene and the *blu*^{tz257} allele. Translated regions are colored black, and untranslated regions are gray. In *blu*^{tz257}, exon 4 is skipped, and the altered reading frame produces a premature stop codon.

blocked completely by glutamate receptor antagonists 6-cyano-7-nitroquinoxaline-2, 3-dione (CNQX) and 2-amino-5-phosphonovalerate (APV), but not by GABA_A receptor antagonist bicuculline (Figure 4A, top), demonstrating that these synapses are exclusively glutamatergic in zebrafish, as they are in other vertebrates. Surprisingly, fairly normal light-evoked responses (Figure 4A, bottom) and action potential-dependent spontaneous EPSCs were observed in the mutants (Figure 4B). Substantial glutamatergic transmission thus remains in the mutant, suggesting that RGCs have additional means to load transmitter into synaptic vesicles, most likely through Vglut1a.

The absence of Vglut2a in *blu* mutant synapses is expected to reduce the number of transporters per vesicle and thus reduce the vesicular concentration of glutamate. To test whether vesicle filling is affected in *blu* mutants, we recorded spontaneous miniature EPSCs (mEPSCs) in the presence of TTX and bicuculline (BMI; Figure 4C). We found a difference in the cumulative amplitude distribution of mEPSCs (Figure 4D) and a reduction in the mean mEPSC amplitude (Figure 4D, inset) in *blu* mutants, consistent with a reduction in vesicular glutamate uptake. The average mEPSC frequency, however, was significantly increased (Figure 4E), suggesting that mutant synapses have an increased probability of release and/or an increased number of release sites. Either of these mechanisms would work to compensate for the reduction in quantal amplitude and thus might account for the relatively normal action potential-evoked EPSCs described above.

The quantal analysis performed above cannot distinguish between presynaptic and postsynaptic effects on mEPSC amplitude. To determine whether the glutamate concentration in the synaptic cleft was reduced in *blu* mutants, we examined the effect of γ -D-glutamylglycine (γ -DGG) on the EPSCs evoked by electrical stimulation of optic fibers. γ -DGG is a low-affinity, fast-dissociating,

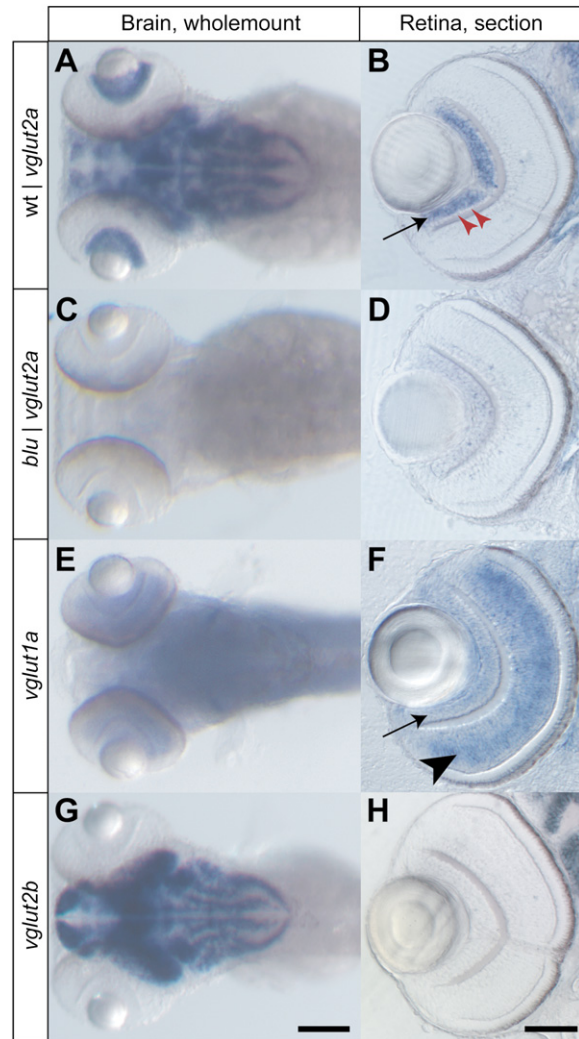


Figure 3. Expression Patterns of Three Zebrafish *vglut* Genes, Detected by RNA In Situ Hybridization

Images in the left column (A, C, E, and G) show whole-mount stainings of the head at 4 dpf, with antisense probes for the genes indicated. The right column (B, D, F, and H) shows vibratome sections (20 μ m) of zebrafish eyes at 4 dpf. (A and B) *vglut2a* is expressed in a complex pattern in the brain of wild-type and in all RGCs in wild-type (arrow). A single row of GABAergic amacrine cells in the RGC layer is negative for *vglut2a* (red arrowheads). (C and D) *vglut2a* RNA (containing a translational stop) is absent in both brain and eye of *blu* mutants. (E and F) *vglut1a* RNA is found in a diffuse pattern in the brain. In the retina, it is strongly expressed in bipolar cells (arrowhead) and weakly in RGCs (arrow). (G and H) *vglut2b* RNA is strongly expressed in a pattern similar to *vglut2a* in the brain and is absent from the retina. Scale bar in (G), 100 μ m (for [A], [C], [E], and [G]); scale bar in (H), 50 μ m (for [B], [D], [F], and [H]).

competitive antagonist for AMPA-type glutamate receptors (Watkins et al., 1990). During a synaptic event, γ -DGG bound to AMPA receptors is replaced by cleft glutamate during the rising phase of the synaptic response, and then bound glutamate is displaced by the antagonist in the falling phase of the response. The efficacy

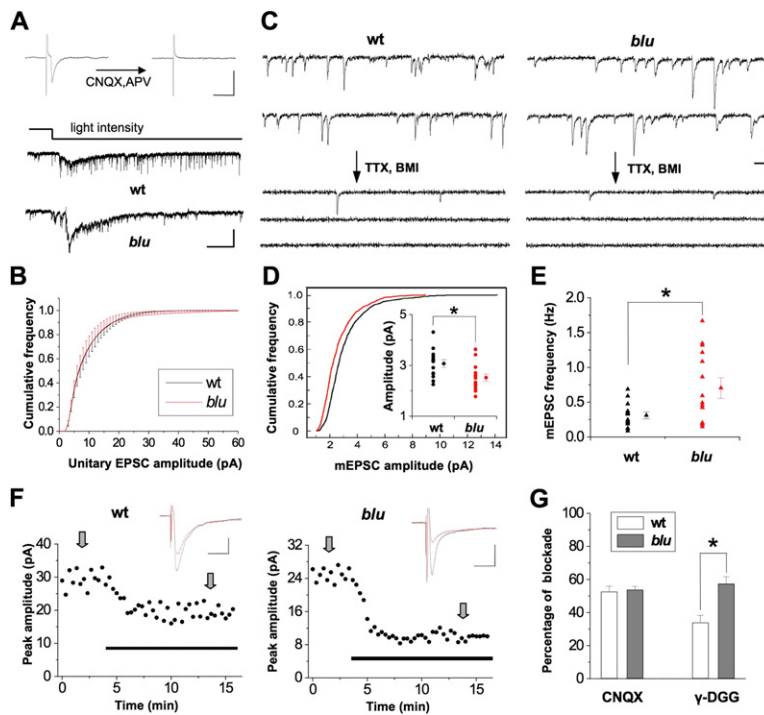


Figure 4. Properties of Retinotectal Synaptic Transmission in *blu* Mutants

(A) (Top) synaptic responses evoked by electrically stimulating optic fibers before and after application of CNQX (10 μ M) and D-APV (25 μ M) to the tectum. Recordings were made at -70 mV and in the presence of 10 μ M bicuculline. Scale: 10 pA, 20 ms. (Bottom) Example tectal cell responses elicited by whole-field dimming stimulus. The time course of change in the light intensity is represented by the top trace. Scale: 20 pA, 1 s.

(B) Average cumulative frequency of the amplitude of unitary EPSCs. Cumulative frequency curves were first made for each cell and then averaged across all cells. Bin size = 1 pA. Wt, $n = 16$ cells; *blu*, $n = 14$ cells.

(C) Example traces of continuous recording of synaptic currents in tectal cells under constant ambient light before and after application of TTX (0.5 μ M) and BMI (10 μ M). Most of the recorded spontaneous events are glutamatergic currents according to their kinetics and reflect action potential-dependent release, since the frequency of miniature EPSCs drops substantially after TTX and BMI application. Scale: 5 pA, 50 ms.

(D) Cumulative distribution of mEPSC amplitudes. 100 mEPSC events were randomly chosen from each cell ($n = 14$ cells in each

group), and the cumulative frequency curve was plotted for the pooled 1400 events. Wt and mutant are significantly different ($p < 0.001$, Kolmogorov-Smirnov test). (Inset) Amplitudes of mEPSCs. Circles on the left in each group represent the average mEPSC amplitudes of individual cells. Average of all cells is shown on the right. The difference is significant ($*p < 0.05$, t test). Black, wt; red, *blu*.

(E) Frequency of mEPSCs. Triangles on the left in each group represent the average mEPSC frequencies of individual cells. The average value in the group is shown by the triangle on the right. The difference is significant ($*p < 0.05$, t test; $n = 14$ cells in each group).

(F) Example experiments in which the peak amplitudes of evoked EPSCs were reduced after bath application of 0.5 mM γ -DGG (indicated by the thick line), in a wild-type cell (left) and a mutant cell (right). EPSCs were evoked by electrical stimulation of the optic fibers, recorded at -70 mV in the presence of picrotoxin (100 μ M). (Top) Average EPSC traces (from eight trials, at times indicated by the arrows) before (black) and after (red) the application of γ -DGG. Scale: 10 pA, 20 ms.

(G) Average percentage of blockade of evoked EPSCs by 0.5 μ M CNQX (left) and 0.5 mM γ -DGG (right). Sample size for CNQX experiments: $n = 7$ cells each from wt and mutant). For γ -DGG experiments, $n = 9$ cells in each group. $*p < 0.01$, t test. Error bars represent SEM.

of displacement of γ -DGG by glutamate depends on its concentration, i.e., the higher concentration of the cleft glutamate, the less inhibition of synaptic responses by γ -DGG (Liu et al., 1999). We compared the amplitudes of evoked EPSCs before and after bath application of 0.5 mM γ -DGG, and of 0.5 μ M CNQX, which is a high-affinity, slow-dissociating antagonist. We found that the level of inhibition of EPSCs by γ -DGG was significantly higher in mutant cells than in wild-type cells, whereas inhibition by CNQX was the same in the two types of cells (Figures 4F and 4G). This suggests that less glutamate is released from RGC axon terminals in mutant fish.

The *blu* Mutation Impairs the Temporal Fidelity of Synaptic Transmission in the Tectum

To gain insight into the dynamics of synaptic transmission under conditions that simulated a temporally changing stimulus, we tested the short-term plasticity of retinotectal synapses. We applied pairs of stimuli, at a range of interstimulus intervals (ISIs) between 50 and 500 ms, and

measured the paired-pulse ratios (PPR), defined as the amplitude of the second EPSC divided by that of the first. Wild-type retinotectal synapses depressed only slightly to paired stimuli delivered at short ISIs. In contrast, mutant synapses showed significantly increased paired-pulse depression, in a strikingly ISI-dependent manner: while the PPRs are similar for mutant and wild-type at the longer ISIs tested (400 ms and greater), a significantly greater depression is seen for mutant synapses at shorter ISIs. The difference of the PPR is most pronounced at an intermediate ISI of 100 ms but curiously disappears for the very shortest ISI measured (50 ms) (Figure 5A). We tested whether this pattern of ISI dependence would also exist for longer trains of stimuli. For trains at an ISI of 100 ms, mutant cells respond with significantly lower amplitude than wild-type throughout the train (Figure 5B). For trains at an ISI of 50 ms, mutant synapses show initially normal responses for the second and sometimes the third pulse, as predicted by the PPR analysis, and are significantly depressed for all subsequent pulses (Figure 5C).

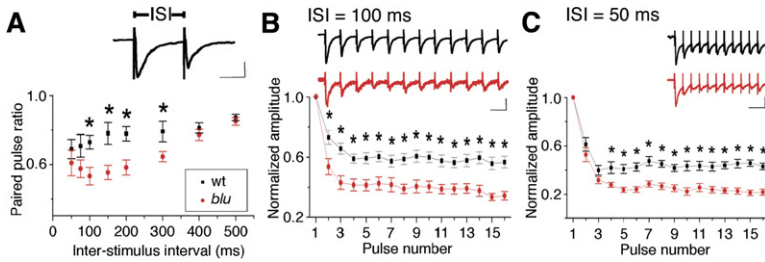


Figure 5. *blu* Mutant Synapses Transmit Deficiently at High Stimulation Rates

(A) Average paired-pulse ratio (amplitude of second response divided by amplitude of first response) at different ISIs. * $p < 0.05$. $n = 10$ cells in each group. (Inset) Example response to paired-pulse stimulus. Scale: 20 pA, 50 ms. (B) Dynamics of synaptic strength during train stimulation. The ISI was 100 ms. The amplitudes of EPSCs were normalized to that of the first response and averaged according to the number of pulses in the train. Bar, SEM. Black, wt ($n = 15$); red, *blu* ($n = 15$). * $p < 0.05$, t test. (Inset) Example responses recorded from a *blu* mutant (red) and a wild-type (black) sibling fish. Scales: 20 pA, 100 ms. (C) Similar presentation except that the ISI was 50 ms. Wt, $n = 10$; *blu*, $n = 12$.

Taken together, our analysis of short-term plasticity demonstrates that *blu* mutant retinotectal synapses are depressed at short pulse intervals (ISI < 400 ms). This reduces the ability of RGC synapses to transmit information at high firing rates (>2.5 Hz), which are evoked in vivo by fast-changing visual stimuli (Bilotta and Abramov, 1989; Hochstein and Shapley, 1976). Strikingly, although perhaps coincidentally, this frequency dependence is in quantitative agreement with the behavioral deficit to high temporal frequency motion (see Figure 1B). We propose that the mutants' failure to detect fast, continuous movements can be explained, at least partially, by premature fatigue of high-frequency synaptic transmission in central visual areas.

Retinotectal Axon Arbors Are Enlarged in the *blu* Mutant

We speculated that the synaptic transmission phenotype could not be used to explain the spatial acuity deficit and that we had to look for an additional structural change of the underlying circuitry. Neural activity has been impli-

cated in the morphological development of RGC axonal arbors (Gnuegge et al., 2001; Hua et al., 2005; Ruthazer et al., 2003; Schmidt et al., 2000). We therefore visualized individual retinal arbors by mosaic expression of a *Brn3c:mGFP* reporter transgene. Individual RGCs were transfected either by DNA plasmid microinjection into one-cell-stage embryos (Tokuoka et al., 2002) or by targeted electroporation (Haas et al., 2002; Hua et al., 2005) of the RGC layer of 2 dpf larvae. Both methods yielded sparse expression of GFP in single or few RGC axons at 7 dpf. Individual RGC arbors ($n = 22$ wild-type and $n = 11$ mutant) were imaged on a laser-scanning confocal microscope (Figure 6A) and analyzed morphometrically by an investigator blind to the genotype (Figure 6B). We found that *blu* mutant arbors were significantly increased in their total branch length (t test, $p < 0.05$) and in their coverage area ($p < 0.01$). The total number of branches also appeared increased in the mutant, but the difference did not reach statistical significance in our sample ($p = 0.25$) (Figures 6C–6E). The expansion in RGC arbor size in *blu* mutants is likely accompanied by an increase in

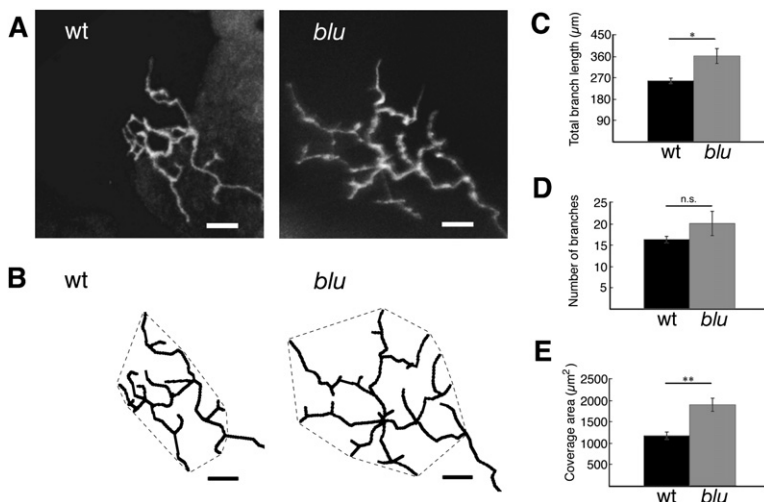


Figure 6. RGC Axon Arbors Are Enlarged in *blu* Mutants

(A) Confocal projections of GFP-labeled RGC axon arbors imaged in vivo at 7 dpf. (B) Arbors were traced in three dimensions from each branch tip to the first branchpoint of the arbor. Tracings were rotated into a plane parallel to the tectal neuropil and projected. Hatched lines around arbors demarcate the coverage area of the arbor. Scale bar: 10 μm . (C–E) Morphometric analysis of RGC axon arbor size reveals that total branch length (C) and coverage area (E) are increased in the mutant. The number of branches (D) is not statistically different. * $p < 0.05$, ** $p < 0.01$. Wt, $n = 22$ cells; *blu*, $n = 11$ cells. Error bar is SEM.

presynaptic release sites and may thus account, at least partially, for the increase in mEPSC frequency described above.

Receptive Fields of Tectal Neurons Are Enlarged in *blu* Mutants

The RF size of visual neurons scales with the convergence of their inputs—the more photoreceptors a given neuron collects input from the larger its RF (Barlow, 1975; Brown et al., 2000; Cleland et al., 1979). In *blu* mutants, each RGC axon arbor may form synapses with a greater number of tectal neurons. Each tectal neuron should then, in turn, receive input from a greater number of RGCs, which collectively sample a larger area of visual space. To test the hypothesis that the mutants' retinal arbor phenotype would enlarge the RFs of their synaptic partners, we measured the visual RFs of tectal neurons. Stimuli were generated on a small LCD screen, using a grid of 8×7 square-shaped pixels, and focused via microscope optics onto the photoreceptor outer segments. Using loose-patch recordings, we measured RFs to the onset (ON RF) and termination (OFF RF) of visual stimulation (Figures 7A–7C).

We found that the mean RF area for *blu* mutants was 60% larger than for wild-type ($p < 0.001$, Kolmogorov-Smirnov test; Figure 7D). This size increase matched the difference in RGC axon arbor area described above. Furthermore, the average spike response per unit stimulus area (i.e., per square in the LCD display) was similar between *blu* mutants and wild-type (Figure 7E). Thus, the local input to tectal neurons is of normal magnitude, suggesting that the reduced glutamatergic drive of individual synapses is compensated by a higher density of synapses on tectal dendrites. Because the presynaptic terminals on a given tectal neuron originate from a greater number of RGCs, individual tectal neurons are stimulated by a larger portion of visual space. An important consequence of this increased convergence is that RFs of neighboring tectal cells will be more overlapping in the mutant, making localization of objects more ambiguous.

blu Mutants Have a Selective Deficit in the Capture of Small Prey, a Tectum-Dependent Behavior

The electrophysiological and anatomical data presented above indicate that vision in *blu* mutants is impaired in a manner that is consistent with behavioral measurements of its perceptual deficits. However, an important caveat of these comparisons is that the OMR does not require retinal input to the tectum, but rather to a different, currently unknown visual area (Roeser and Baier, 2003). Because *vglut2a* is expressed in all RGCs, it is reasonable to assume that synaptic properties, particularly the kinetics of transmitter release, are similar across the entire RGC population. Nevertheless, the deficits in OMR cannot be matched up directly with the retinotectal phenotypes. We therefore decided to investigate another behavior, prey capture, which is largely visually mediated and dependent on the tectum (Gahtan et al., 2005).

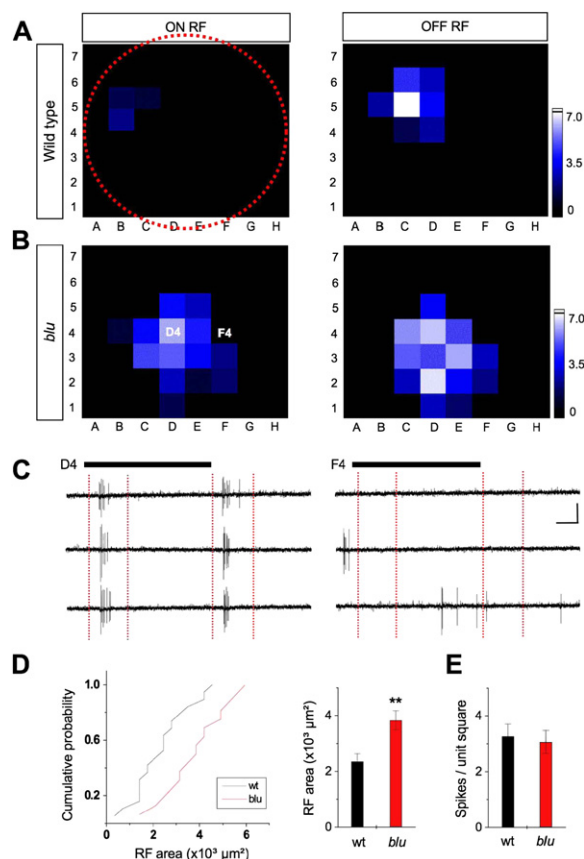


Figure 7. Receptive Fields of Tectal Neurons Are Enlarged in *blu* Mutant

(A) Example of an ON (left) and OFF (right) RF from a 7 dpf wild-type larva. The red-dotted circle depicts the relative size of the entire visual field (retinal surface).

(B) Example RF from a 7 dpf *blu* mutant. The brightness of each unit in the 56 square grid represents the average number of spikes (three repetitions) evoked by the corresponding stimulus. See scale on the right.

(C) Response traces of three repetitions are shown for stimulus position in D4 (left) and F4 (right) in the example shown in (B). ON and OFF RFs are analyzed within time windows (red vertical dashed lines) that cover ON responses and OFF responses, respectively. Black bars represent the duration of the stimulus (1.5 s). Scales: 20 pA, 250 ms.

(D) (Left) Cumulative distribution of RF sizes (number of squares showing spike responses, multiplied by $350 \mu\text{m}^2$). (Right) Average RF area. RFs in *blu* mutants are, on average, 60% larger than in wt. ** $p < 0.001$, Kolmogorov-Smirnov test. Wt, $n = 19$; *blu*, $n = 16$.

(E) Average number of spikes per square unit within the RF. Local input strength is similar between *blu* and wt. Error bars are SEM.

Larval zebrafish pursue, catch, and eat paramecia (Figure 8A). We asked whether *blu* mutants have a spatial acuity deficit for prey capture. Two species of *Paramecium* were used, which differ in size. *P. multimicronucleatum* are about $200\text{--}350 \mu\text{m}$ in length, while *P. aurelia* are $120\text{--}180 \mu\text{m}$ (see Protist Information Server at <http://taxa.soken.ac.jp/www/>). In our assay, fish were placed in a small Petri dish, each with 20 to 100 paramecia. At varying time intervals thereafter, the paramecia remaining

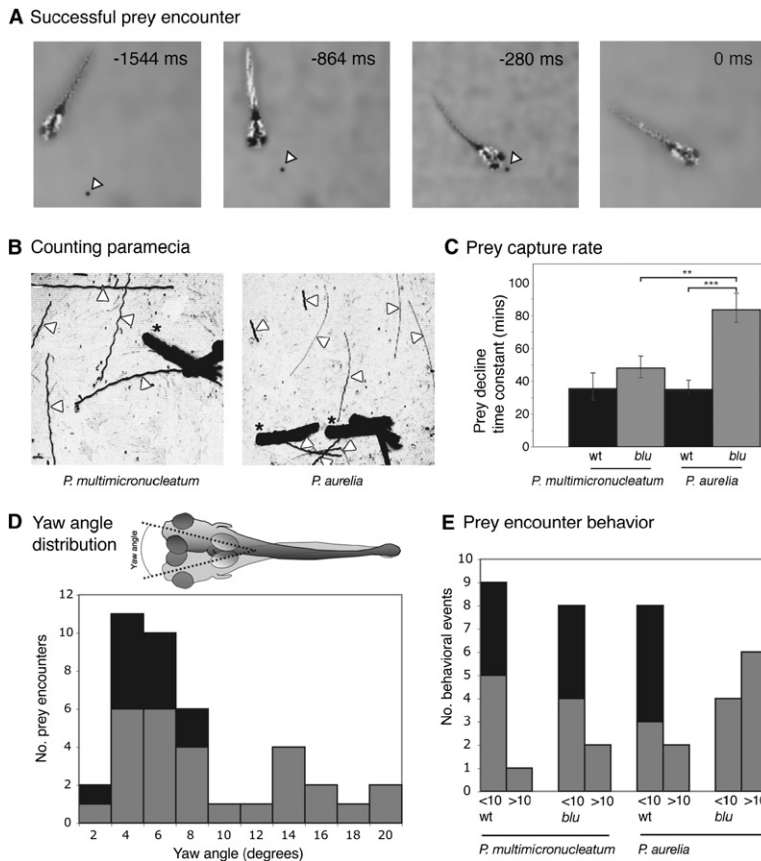


Figure 8. Prey Capture by *blu* Mutants Has Reduced Spatial Resolution

(A) Still frames from a recording of a successful prey-capture event. Time stamps give the time in ms before capture. Paramecia (black dots marked by white arrowheads) have been contrast enhanced for display purposes.

(B) Example images used to quantify prey capture. Zebrafish larvae (thick black silhouettes, marked by asterisks) are placed in small Petri dishes with 20 to 100 paramecia. The number of paramecia remaining in the dish is monitored over time from 4 s movies, which reveal their thin, straight swimming trajectories (open arrowheads). The small species (*P. aurelia*, right) often leaves thinner, but equally long, streaks than the big species (*P. multimicronucleatum*, left).

(C) Mutants are impaired in capturing *P. aurelia*, but consume *P. multimicronucleatum* at almost normal rates. Error bars are the 95% confidence interval for the estimate of the time constant. *P. aurelia*, wt, n = 23 dishes; *blu*, n = 24 dishes. *P. multimicronucleatum*, wt, n = 14 dishes; *blu*, n = 15 dishes. Statistical significance was determined with an F test. **p < 0.01, ***p < 0.001.

(D) Head yaw angle distribution histogram in all 40 prey encounters recorded. The inset shows a cartoon of the superimposed silhouettes of a fish at two time points. Head yaw angles below 10° correspond to orienting swims, and angles greater than 10° correspond to routine swims. Almost half of the orienting swims resulted in successful prey captures (black segments).

(E) Distribution of orienting swims (<10°) and routine swims (>10°) during prey encounters, analyzed across genotype and prey species (n = 10 each). Black segments indicate successful prey captures. *blu* mutants execute fewer orienting swims in encounters with *P. aurelia*.

in the dish were counted (Figure 8B; see [Experimental Procedures](#)). These data were fitted with an exponential function, derived from the Lotka-Volterra differential equations, assuming a steady rate of consumption of prey by a constant number of predators (see [Experimental Procedures](#)). The time constant of prey decline is inversely related to the efficiency of prey capture.

We found that *blu* mutants consumed the large species, *P. multimicronucleatum*, at the same rate as wild-type siblings (wt, n = 14 dishes; *blu*, n = 15 dishes), demonstrating that the mutation did not disrupt the fishes' appetite or locomotor capabilities (Figure 8C; F test, p > 0.5). In contrast, the mutants took much longer than wild-type to capture the smaller species, *P. aurelia* (p < 0.001; wt, n = 21 dishes; *blu*, n = 23 dishes). Thus, while wild-type fish consumed the two species with similar speeds, *blu* mutants were significantly less efficient in catching *P. aurelia* than *P. multimicronucleatum* (p < 0.01). The two species of paramecia did not differ in their swimming speeds (note the lengths of the longest swimming trajectories in Figure 8B) and are

unlikely to differ in their ability to evade capture. Therefore, the most likely explanation for the mutant's greater difficulty in catching *P. aurelia* is a deficiency in visual acuity, which makes the smaller species harder to detect.

To further confirm that *blu* mutants' deficit in capturing *P. aurelia* was due to an impairment in visual detection and not a deficit in motor coordination or in the ability to hold the small paramecia in their mouths, we analyzed individual prey-encounter events. Previous studies have shown that zebrafish prey-capture swims can be distinguished from routine swims on the basis of several kinematic criteria (Borla et al., 2002; Gahtan et al., 2005). Most prominently, during prey-capture swims, the fish reduce the head yaw angle of their swims relative to their routine swims (Figure 8D). Prey-capture swims are characterized by yaw angles less than 10°, whereas for routine swims the yaw angle is greater than 10° (Gahtan et al., 2005). This criterion can therefore be used to determine whether a zebrafish larva has detected the prey, before the actual capture occurs. Our data demonstrated that

blu mutants executed the low yaw-angle swims less often when encountering the small paramecia, whereas they entered the low yaw-angle swim mode at normal frequency when encountering the larger species (Figure 8E). This finding demonstrated that their deficit lies in the sensory detection of small prey. Since paramecium capture at this larval age is almost completely dependent on vision and, more specifically, the tectum (Gahtan et al., 2005), the defect most likely lies in the retinotectal system. Together, these results support our hypothesis that the enlargement of RGC axon arbors degrades the fine spatial structure of visual information as it is transmitted to the tectum.

DISCUSSION

The zebrafish *blu* mutant was initially discovered in a forward-genetic screen for retinotectal mutants and later shown to have impairments in visual behavior (Baier et al., 1996; Neuhauss et al., 1999; Trowe et al., 1996). We show here by positional cloning that the *blu* gene encodes Vglut2a, a member of the vesicular glutamate transporter gene family, which mediates the uptake of glutamate by presynaptic vesicles (Bellocchio et al., 2000; Takamori et al., 2001). The *vglut2a* gene is expressed in all RGCs, but is not detectable in glutamatergic neurons presynaptic to RGCs. Thus, the synapses formed by retinofugal axons in central areas are the first in the visual pathway to be affected by the absence of this transporter. Given the bottleneck function of RGCs in visual processing, the deficits in behavioral responses observed here are likely due to changes in synaptic transmission from RGCs to neurons in the tectum and other retinorecipient nuclei. Our own localization studies and those of others (Higashijima et al., 2004) have shown that *vglut2a* is also expressed in other areas of the CNS. It will be interesting to investigate in the future how this mutation affects other behavioral functions beyond the visual system. We expect the strongest effects on synapses where expression of *vglut2a* does not overlap with that of either *vglut1a* or *vglut2b*.

We asked how the absence of Vglut2a affected retinotectal transmission. Recordings from tectal neurons, which receive synaptic input from RGCs, showed that substantial glutamatergic transmission remains in the mutant. We considered the possibility that the *blu*^{tz257} allele might be a hypomorph, and mutant Vglut2a may retain some transport activity. However, two pieces of evidence argue against this interpretation. First, the mutation is in a nucleotide necessary for splicing, and the resultant splicing error creates a premature stop codon. As a result of this base pair change, the mutant mRNA lacks an exon, and the mutant protein is expected to be truncated to less than a third of its normal length, lacking several transmembrane domains (Fremeau et al., 2001). Second, *vglut2a* mRNA is undetectable in *blu* mutants, probably due to nonsense-mediated RNA decay. Thus, protein may not even be made at all in the mutant. A more likely explana-

tion for the mildness of the phenotype is that vesicular glutamate uptake in zebrafish RGCs is only partially dependent on Vglut2a. Five other members of the *vglut* gene family are present in the zebrafish genome, and of these, we found *vglut1a* to be weakly expressed in RGCs. Thus, although none of the other *vglut* family members tested appears to be upregulated in *blu* mutants, at least Vglut1a is present in RGCs, where it could serve a partially redundant function in vesicular glutamate transport.

Although synaptic transmission is grossly normal in *blu* mutants, our further analyses revealed several deficits. First of all, mEPSC amplitudes are smaller, consistent either with a reduction of vesicular glutamate uptake in the mutant or with a reduced number of postsynaptic receptors. To narrow down these possibilities, we measured the blockade of evoked EPSCs by the low-affinity, fast-dissociating AMPA receptor antagonist γ -DGG (Liu et al., 1999). EPSCs were blocked to a greater extent in mutants than in wild-type by γ -DGG, while the high-affinity antagonist CNQX showed no difference. This result demonstrated that glutamate concentration in the synaptic cleft is indeed reduced in *blu* mutants. Additional changes on the postsynaptic side cannot be excluded from this experiment. Previous studies of autaptic cultures of hippocampal neurons from *vglut1* mutant mice (Wojcik et al., 2004) and overexpression experiments at the *Drosophila* neuromuscular junction (Daniels et al., 2004) have shown that quantal amplitude is directly related to the number of transporter molecules. In apparent contrast to these results, mEPSC amplitudes remained unaltered in hippocampal slice recordings from *vglut1* null mice (Fremeau et al., 2004). This finding is due to the coexpression of Vglut1 and Vglut2, which segregate to distinct populations of synaptic sites in these neurons. Although we cannot exclude a similar segregation principle at retinotectal synapses, our data are most parsimoniously explained by colocalization of the Vglut isoforms Vglut2a and Vglut1a in the same vesicle.

Second, we found that mEPSC frequency is increased in our mutant. This change may be due either to an increase in the probability of release and/or to an increase in the number of release sites.

Third, we found that evoked EPSCs are depressed to a significantly larger degree in the mutant when pulses are applied at high rates. The difference is not seen at pulse intervals greater than 400 ms. Paired-pulse depression could be due to depletion of the readily releasable pool of vesicles—synapses with higher release probability tend to show a reduced PPR (Zucker and Regehr, 2002). In *blu* mutants, a single pulse may deplete the readily releasable pool of vesicles enough to cause increased depression to the second pulse. Such an effect could be caused by a reduced number of vesicles at each synapse, as has been reported in Vglut1 knockout mice (Fremeau et al., 2004). Alternatively or in addition, recently recycled vesicles might take longer to refill, in agreement with the presence of fewer transporters per vesicle (Gasnier, 2000). When these vesicles are recruited to respond to

the second pulse, they would contain less glutamate and thus would lower the amplitude of the second response. Whatever the exact cause of the depression, our results led us to predict that processing of visual information should show selective fatigue in tasks that require high RGC firing rates.

The synaptic deficits in the *blu* mutant also indirectly compromise the precision of the retinotectal map. During embryonic development (in zebrafish beginning shortly after 2 dpf), RGC axons project into the superficial layers of the contralateral tectum in retinotopic order, i.e., preserving the neighborhood relationships of their cell bodies in the retina (Johnson and Harris, 2000; McLaughlin et al., 2003). In *blu* mutants, previous Dil-labeling studies had shown that, while coarse retinotopy was intact, the termination zones of small groups of RGC axons appeared more dispersed in the tectum (Trowe et al., 1996). By single-axon tracing, we are now able to attribute this multi-axon phenotype to the expansion of individual arbors. Larger arbors may accommodate more presynaptic active zones, a hypothesis consistent with the observed increase in mEPSC frequency. An increased number of synaptic contacts could thus explain the rather mild electrophysiological deficits observed in the mutant.

Retinal arbor size can be influenced by activity-dependent processes, such as competitive interactions with neighboring axons and Hebbian plasticity (Hua and Smith, 2004; Ruthazer et al., 2003). More directly, glutamate released from the presynaptic terminals has been reported to inhibit axon growth (Kreibich et al., 2004). The evidence, however, suggests a different explanation, which has not been proposed previously (to our knowledge) for the retinotectal system. We propose that axon growth is part of a homeostatic response to lowered synaptic activity. First, glutamatergic drive per tectal neuron is normalized in the mutant, arguing for a finely tuned homeostatic mechanism and against unregulated, exuberant growth. Second, in preliminary transplantation studies, we showed that mutant RGC arbors were normal-sized when surrounded by wild-type axons, excluding a cell-autonomous effect of reduced glutamate release on arbor growth (M.C.S. and H.B., unpublished data). Third, all RGC axons are equally, or at least similarly, affected by the absence of functional Vglut2a; competition through varying activity levels is therefore unlikely to account for increases in arbor size (Hua et al., 2005). Fourth, treatment with MK-801, a blocker of glutamate receptors of the NMDA subtype, leads to a similar enlargement of RGC arbors in wild-type (Schmidt et al., 2000), suggesting that addition of synapses may be a general response to reduction of synaptic transmission in the zebrafish retinotectal system. We therefore propose a homeostatic signaling mechanism by which the postsynaptic cell promotes growth of the presynaptic arbor to compensate for reduced synaptic drive (Burrone and Murthy, 2003; Davis and Bezprozvanny, 2001).

Our findings complement those of Hua et al. (2005), who found evidence for a role of activity-based competition in

regulating axon arbor growth. In this study, inactive axons, in which either action potentials or vesicle fusions were blocked by overexpression of Kir2.1 or a dominant-negative VAMP (VAMPm), respectively, were smaller than their active neighbors. However, no change in arbor size was seen when all axons were uniformly inactivated (Hua et al., 2005). This confirmed earlier studies in zebrafish, which had also been unable to detect changes in arbor size after global activity blockage (Gnuegge et al., 2001; Stuermer et al., 1990). In apparent contrast to these studies, we found that Vglut2a-deficient arbors are larger than wild-type axons. One difference between the effects of the *blu* mutation and those of Kir2.1 or VAMPm overexpression is the degree of blockage. While Kir2.1 largely inhibits spiking, and VAMPm is likely to abolish synaptic exocytosis, the perturbation caused by absence of Vglut2a is much milder. Another notable difference between the two experiments is the cellular process that was inhibited: Hua et al. (2005) impeded synaptic transmission upstream of the *blu* mutant's defect in vesicular glutamate uptake, while excitability and exocytosis should be normal, or nearly so, in *blu* mutants. Our results, taken together with those of Hua et al. (2005), suggest that neural activity may sculpt RGC axon arbors through both competition and homeostasis. The relative prevalence of these two mechanisms may depend on the degree of differences in the levels of presynaptic activity and/or the cellular substrates of the synaptic deficiency.

Just as temporal resolution of vision is limited by the kinetics of phototransduction (Baylor, 1996), it should also depend on the properties of synaptic transmission further downstream in the visual system. Rapid modulation of visual stimuli results in higher firing rates in RGCs (Bilotta and Abramov, 1989; Hochstein and Shapley, 1976). The short-term depression we see in *blu* mutants should function as a low-pass filter on the transfer of information across synapses (Fortune and Rose, 2001; Tsodyks and Markram, 1997). We found that gratings that move at high temporal frequencies were indeed less visible to the mutants. The temporal frequency range in which the mutants showed an impairment (>2.5 Hz) is in striking agreement with the interstimulus-interval range (<400 ms) in which their retinotectal synapses showed increased depression to repetitive stimulation.

The neural substrate underlying acute spatial vision has rarely been explored outside of primates and has not been identified experimentally for any species. While the spacing of photoreceptors puts physical limits on visual acuity in the primate fovea (Geisler, 1984; Hirsch and Hylton, 1984; Williams and Coletta, 1987), perceptual thresholds outside the fovea correlate with the RFs of RGCs (Banks et al., 1991; Barlow, 1975; Enroth-Cugell and Robson, 1966; Jacobs and Blakemore, 1988; Kiorpes and Movshon, 2003). In young zebrafish larvae, the theoretical resolution limit set by intercone distances, the Nyquist frequency, is greater than 0.34 cycles/° (less than 3° of the visual field) after 4 dpf (Easter and Nicola, 1996), while grating acuity does not exceed 0.16 cycles/° (6°) at 5–7

dpf in wild-type (Rinner et al., 2005). Because RGC axon arbors are larger and more overlapping in *blu* mutants, a given postsynaptic target neuron is likely to receive synaptic input from a larger number of RGCs spread over a greater area within the retina. Here we have shown that tectal RF areas are increased by 60% on average. The mutants were indeed less able to detect fine gratings in the OMR assay, even when the drift velocity was very slow. In addition, we tested visually guided prey capture, a tectum-dependent behavior (Gahtan et al., 2005). We find that *blu* mutants were less able to detect and to catch a small prey species (*Paramecium aurelia*) than a prey species twice as large (*Paramecium multimicronucleatum*). These experiments point to the retinotectal neuropil as an important processing station where synaptic architecture can limit spatial acuity.

Our physiological, anatomical, and behavioral investigations into the zebrafish *blu/vglut2a* mutant demonstrate a tight correspondence between specific perceptual abilities and the arrangement and function of the underlying synaptic circuitry. The most parsimonious interpretation of these results is that resolution of fast-changing visual scenes depends on rapid recovery of synaptic transmission, while high-acuity spatial vision requires precise retinotopic mapping. It is noteworthy that the primary physiological deficit of the mutant (reduced synaptic drive) seems to precipitate secondary physiological and anatomical changes (increased synapse number and, possibly, increased probability of release), which largely compensate for the initial perturbation. Homeostatic regulation may thus account for the relatively normal postsynaptic responses, but it comes at the expense of visual acuity. Our study has revealed a likely causal link between a molecular defect and a change in visual perception and behavior.

EXPERIMENTAL PROCEDURES

Optomotor Response Assay

The OMR was tested as previously described (Orger et al., 2000). See the Supplemental Data for details. All measurements are an average of the response of at least 12 tanks. For motion-nulling experiments, stimuli consisted of a 10% contrast, 0.012 cycles/degree, 0.93 Hz grating stimulus, moving in one direction (the reference stimulus), superimposed on a stimulus of variable spatial and temporal frequency (the test stimulus), moving in the opposite direction. For the test stimulus, the contrast varied from 0, which evoked a response from the fish in the direction of the reference stimulus, to a contrast at which the test stimulus overrode the reference stimulus. For each test stimulus, a contrast just below and just above that necessary to change the direction of the OMR were repeated, and the zero-crossing point of the line connecting them was taken as the null point.

Positional Cloning, Genotyping, and RNA In Situ Hybridization

We used established procedures for linkage mapping and sequencing of candidate genes. For detailed information, see the Supplemental Data. Mutants older than 5 dpf could be readily identified by their abnormally dark coloration. This phenotype is due to a deficit in a retina-dependent neuroendocrine response, in which melanosome distribution is regulated by ambient light levels. Some zebrafish visual mutants have this phenotype (Muto et al., 2005; Neuhauss et al., 1999). Mutant

larvae younger than 5 dpf were genotyped using a mismatch PCR-RFLP strategy, in which a restriction site was added to amplified genomic sequence using a primer containing additional bases adjacent to the site of the *blu* mutation. The primer sequence added an MbolI site to the mutant allele, which was absent from the wild-type allele.

Whole-mount RNA in situ hybridization was performed similar to Keegan et al., 2002. For sequence information and details of the procedure, see Supplemental Data.

Tectal Cell Electrophysiology

Larval fish at 5–8 dpf were anesthetized with saline containing 0.02% MS222, secured by insect pins to a sylgard-coated dish, and incubated in the recording medium containing (in mM): 134 NaCl, 2.9 KCl, 2.1 CaCl₂, 1.2 MgCl₂, 10 HEPES, 10 glucose (pH 7.6). The skin over the brain was removed, and the brain was split open along the midline to expose the tectum. Tectal cells were patched under visual control, as described in Supplemental Data.

Receptive Field Mapping

Larvae (7–8 dpf) were used. The lens of the contralateral eye was removed to expose the retina. The retina was then flattened and stabilized with a small piece of glass coverslip. A small LCD screen (Sony, PLM-A35) was mounted on the camera port of a microscope, allowing projection of computer-generated images onto the retina. To measure RF size, a loose-patch recording from a tectal cell was established under visual control. For stimulation, the microscope was then moved with manipulators while the stage remained stationary, and the microscope was refocused on the retina. Visual stimuli were programmed with LabVIEW software. The entire image covered >90% of the retinal surface and was divided into an 8 × 7 grid of 56 square units. White squares (corresponding to one of the 56 units in the grid) on a black background were flashed for 1.5 s in a pseudorandom sequence, separated by 2 s intervals. RFs were mapped for three repetitions. Each unit stimulus covered 350 μm². The entire retina was about 17,600 μm². There was no significant difference in the retina size among individuals. Custom-written LabVIEW codes were used to analyze RFs. ON or OFF responses were analyzed within a 600 ms time window, starting 50 ms after the onset or offset of the stimulus, respectively (to account for the latency of the phototransduction cascade). A unit square was identified as “responsive” if at least one spike was evoked in all three repetitions. In the color map of Figure 7, brightness represents the average number of spikes from these repetitions. RF area is calculated by multiplying the number of “responsive” square units by 350 μm² (the projected square area on the retina). In wild-type, RFs were between 2 and 13 squares large. RF strength (spikes per RF area) was calculated by dividing the total number of spikes elicited by all stimuli within the RF by the number of “responsive” squares. Tectal neurons may exhibit exclusively ON responses, exclusively OFF responses, or both ON and OFF responses. In the latter case, the strongest response was included for the quantification.

Single Axon Arbor Analysis

Six kb of sequence upstream of the zebrafish *brn3c* gene was cloned upstream of the Gal4 transcription factor. The same plasmid contained a membrane-targeted GFP (Kay et al., 2004) under control of the Gal4 upstream activating sequence (UAS). The *Brn3c:Gal4; UAS:mGFP* construct was incorporated into RGCs by single-cell electroporation (Haas et al., 2002; Hua et al., 2005). At 7 dpf, larvae were embedded in 1% agarose and imaged on a Bio-Rad MRC 1024 confocal microscope. For details of the morphometric analysis, see the Supplemental Data.

Prey-Capture Assay

Prey capture was assayed as previously described (Gahtan et al., 2005). *Paramecium multimicronucleatum* and *Paramecium aurelia* were obtained from Carolina Biological Supplies (Burlington, NC). For details of the procedure, see Supplemental Data.

Supplemental Data

The Supplemental Data for this article can be found online at <http://www.neuron.org/cgi/content/full/53/1/65/DC1/>.

ACKNOWLEDGMENTS

We thank S. Higashijima, G. Mandel, and J. Fetcho (SUNY, Stony Brook) for generously providing us with the RNA probes against zebrafish *vglut* genes prior to publication. We thank D. Stainier for the use of his PAC library. Ann Wehman suggested the RFLP method used to genotype *blu*. We thank M. Stryker, D. Copenhagen, C. Bargmann, R. Edwards, R. Fremneau, K. Kam, M. Carey, K. Menuz, and members of the Baier lab, especially A. Wehman and P. Page-McCaw, for discussions and comments on the manuscript. H-z.W.T. thanks Li Zhang for discussions and his long-term support. This work was largely funded by NIH EY12406, an Esther and Joseph Klingenstein Fellowship, and a David and Lucile Packard Fellowship (H.B.). H-z.W.T. and M.-m.P. were partially supported by NIH EY014979. M.C.S. was supported by an NSF Predoctoral Fellowship, by a UCSF Chancellor's Fellowship, and by the American Heart Association. M.B.O. was supported by a Howard Hughes Predoctoral Fellowship. N.J.G. was supported by an NRSA Predoctoral Fellowship.

Received: March 23, 2006

Revised: October 30, 2006

Accepted: December 13, 2006

Published: January 3, 2006

REFERENCES

- Baier, H., Klostermann, S., Trowe, T., Karlstrom, R.O., Nusslein-Volhard, C., and Bonhoeffer, F. (1996). Genetic dissection of the retinotectal projection. *Development* **123**, 415–425.
- Banks, M.S., Sekuler, A.B., and Anderson, S.J. (1991). Peripheral spatial vision: limits imposed by optics, photoreceptors, and receptor pooling. *J. Opt. Soc. Am. A* **8**, 1775–1787.
- Barlow, H.B. (1975). Visual experience and cortical development. *Nature* **258**, 199–204.
- Baylor, D. (1996). How photons start vision. *Proc. Natl. Acad. Sci. USA* **93**, 560–565.
- Bellocchio, E.E., Reimer, R.J., Fremneau, R.T., Jr., and Edwards, R.H. (2000). Uptake of glutamate into synaptic vesicles by an inorganic phosphate transporter. *Science* **289**, 957–960.
- Bilotta, J., and Abramov, I. (1989). Spatial properties of goldfish ganglion cells. *J. Gen. Physiol.* **93**, 1147–1169.
- Borla, M.A., Palecek, B., Budick, S., and O'Malley, D.M. (2002). Prey capture by larval zebrafish: evidence for fine axial motor control. *Brain Behav. Evol.* **60**, 207–229.
- Brown, S.P., He, S., and Masland, R.H. (2000). Receptive field microstructure and dendritic geometry of retinal ganglion cells. *Neuron* **27**, 371–383.
- Burrone, J., and Murthy, V.N. (2003). Synaptic gain control and homeostasis. *Curr. Opin. Neurobiol.* **13**, 560–567.
- Chichilnisky, E.J., Heeger, D., and Wandell, B.A. (1993). Functional segregation of color and motion perception examined in motion nulling. *Vision Res.* **33**, 2113–2125.
- Cleland, B.G., Harding, T.H., and Tulunay-Keesey, U. (1979). Visual resolution and receptive field size: examination of two kinds of cat retinal ganglion cell. *Science* **205**, 1015–1017.
- Daniels, R.W., Collins, C.A., Gelfand, M.V., Dant, J., Brooks, E.S., Krantz, D.E., and DiAntonio, A. (2004). Increased expression of the *Drosophila* vesicular glutamate transporter leads to excess glutamate release and a compensatory decrease in quantal content. *J. Neurosci.* **24**, 10466–10474.
- Davis, G.W., and Bezprozvanny, I. (2001). Maintaining the stability of neural function: a homeostatic hypothesis. *Annu. Rev. Physiol.* **63**, 847–869.
- Easter, S.S., Jr., and Nicola, G.N. (1996). The development of vision in the zebrafish (*Danio rerio*). *Dev. Biol.* **180**, 646–663.
- Engert, F., Tao, H.W., Zhang, L.I., and Poo, M.M. (2002). Moving visual stimuli rapidly induce direction sensitivity of developing tectal neurons. *Nature* **419**, 470–475.
- Enroth-Cugell, C., and Robson, J.G. (1966). The contrast sensitivity of retinal ganglion cells of the cat. *J. Physiol.* **187**, 517–552.
- Fortune, E.S., and Rose, G.J. (2001). Short-term synaptic plasticity as a temporal filter. *Trends Neurosci.* **24**, 381–385.
- Fremneau, R.T., Jr., Troyer, M.D., Pahner, I., Nygaard, G.O., Tran, C.H., Reimer, R.J., Bellocchio, E.E., Fortin, D., Storm-Mathisen, J., and Edwards, R.H. (2001). The expression of vesicular glutamate transporters defines two classes of excitatory synapse. *Neuron* **31**, 247–260.
- Fremneau, R.T., Jr., Kam, K., Qureshi, T., Johnson, J., Copenhagen, D.R., Storm-Mathisen, J., Chaudhry, F.A., Nicoll, R.A., and Edwards, R.H. (2004). Vesicular glutamate transporters 1 and 2 target to functionally distinct synaptic release sites. *Science* **304**, 1815–1819.
- Gahtan, E., Tanger, P., and Baier, H. (2005). Visual prey capture in larval zebrafish is controlled by identified reticulospinal neurons downstream of the tectum. *J. Neurosci.* **25**, 9294–9303.
- Gasnier, B. (2000). The loading of neurotransmitters into synaptic vesicles. *Biochimie* **82**, 327–337.
- Geisler, W.S. (1984). Physical limits of acuity and hyperacuity. *J. Opt. Soc. Am. A* **1**, 775–782.
- Gnuegge, L., Schmid, S., and Neuhauss, S.C. (2001). Analysis of the activity-deprived zebrafish mutant macho reveals an essential requirement of neuronal activity for the development of a fine-grained visuotopic map. *J. Neurosci.* **21**, 3542–3548.
- Haas, K., Jensen, K., Sin, W.C., Foa, L., and Cline, H.T. (2002). Targeted electroporation in *Xenopus* tadpoles in vivo—from single cells to the entire brain. *Differentiation* **70**, 148–154.
- Higashijima, S., Mandel, G., and Fetcho, J.R. (2004). Distribution of prospective glutamatergic, glycinergic, and GABAergic neurons in embryonic and larval zebrafish. *J. Comp. Neurol.* **480**, 1–18.
- Hirsch, J., and Hylton, R. (1984). Quality of the primate photoreceptor lattice and limits of spatial vision. *Vision Res.* **24**, 347–356.
- Hochstein, S., and Shapley, R.M. (1976). Quantitative analysis of retinal ganglion cell classifications. *J. Physiol.* **262**, 237–264.
- Hua, J.Y., and Smith, S.J. (2004). Neural activity and the dynamics of central nervous system development. *Nat. Neurosci.* **7**, 327–332.
- Hua, J.Y., Smear, M.C., Baier, H., and Smith, S.J. (2005). Regulation of axon growth in vivo by activity-based competition. *Nature* **434**, 1022–1026.
- Jacobs, D.S., and Blakemore, C. (1988). Factors limiting the postnatal development of visual acuity in the monkey. *Vision Res.* **28**, 947–958.
- Johnson, K.G., and Harris, W.A. (2000). Connecting the eye with the brain: the formation of the retinotectal pathway. *Results Probl. Cell Differ.* **31**, 157–177.
- Kay, J.N., Roeser, T., Mumm, J.S., Godinho, L., Mrejeru, A., Wong, R.O., and Baier, H. (2004). Transient requirement for ganglion cells during assembly of retinal synaptic layers. *Development* **131**, 1331–1342.
- Keegan, B.R., Feldman, J.L., Lee, D.H., Koos, D.S., Ho, R.K., Stainier, D.Y., and Yelon, D. (2002). The elongation factors Pandora/Spt6 and Foggy/Spt5 promote transcription in the zebrafish embryo. *Development* **129**, 1623–1632.
- Kiorpes, L., and Movshon, J.A. (2003). Neural limitations on visual development in primates. In *The Visual Neurosciences*, L.M. Chalupa and J.S. Werner, eds. (Cambridge, MA: MIT Press), pp. 234–259.

- Kreibich, T.A., Chalasani, S.H., and Raper, J.A. (2004). The Neurotransmitter glutamate reduces axonal responsiveness to multiple repellents through the activation of metabotropic glutamate receptor 1. *J. Neurosci.* *24*, 7085–7095.
- Liu, G., Choi, S., and Tsien, R.W. (1999). Variability of neurotransmitter concentration and nonsaturation of postsynaptic AMPA receptors at synapses in hippocampal cultures and slices. *Neuron* *22*, 395–409.
- McLaughlin, T., Hindges, R., and O'Leary, D.D. (2003). Regulation of axial patterning of the retina and its topographic mapping in the brain. *Curr. Opin. Neurobiol.* *13*, 57–69.
- Muto, A., Orger, M.B., Wehman, A.M., Smear, M.C., Kay, J.N., Page-McCaw, P.S., Gahtan, E., Xiao, T., Nevin, L.M., Gosse, N.J., et al. (2005). Forward genetic analysis of visual behavior in zebrafish. *PLoS Genetics* *1*, e66. 10.1371/journal.pgen.0010066.
- Neuhauss, S.C. (2003). Behavioral genetic approaches to visual system development and function in zebrafish. *J. Neurobiol.* *54*, 148–160.
- Neuhauss, S.C., Biehlmaier, O., Seeliger, M.W., Das, T., Kohler, K., Harris, W.A., and Baier, H. (1999). Genetic disorders of vision revealed by a behavioral screen of 400 essential loci in zebrafish. *J. Neurosci.* *19*, 8603–8615.
- Orger, M.B., and Baier, H. (2005). Channeling of red and green cone inputs to the zebrafish optomotor response. *Vis. Neurosci.* *22*, 275–281.
- Orger, M.B., Smear, M.C., Anstis, S.M., and Baier, H. (2000). Perception of Fourier and non-Fourier motion by larval zebrafish. *Nat. Neurosci.* *3*, 1128–1133.
- Reid, R.C., and Alonso, J.M. (1995). Specificity of monosynaptic connections from thalamus to visual cortex. *Nature* *378*, 281–284.
- Rinner, O., Rick, J.M., and Neuhauss, S.C. (2005). Contrast sensitivity, spatial and temporal tuning of the larval zebrafish optokinetic response. *Invest. Ophthalmol. Vis. Sci.* *46*, 137–142.
- Roeser, T., and Baier, H. (2003). Visuomotor behaviors in larval zebrafish after GFP-guided laser ablation of the optic tectum. *J. Neurosci.* *23*, 3726–3734.
- Ruthazer, E.S., Akerman, C.J., and Cline, H.T. (2003). Control of axon branch dynamics by correlated activity in vivo. *Science* *301*, 66–70.
- Schmidt, J.T., Buzzard, M., Borress, R., and Dhillon, S. (2000). MK801 increases retinotectal arbor size in developing zebrafish without affecting kinetics of branch elimination and addition. *J. Neurobiol.* *42*, 303–314.
- Shimoda, N., Knapik, E.W., Ziniti, J., Sim, C., Yamada, E., Kaplan, S., Jackson, D., de Sauvage, F., Jacob, H., and Fishman, M.C. (1999). Zebrafish genetic map with 2000 microsatellite markers. *Genomics* *58*, 219–232.
- Stuermer, C.A. (1988). Retinotopic organization of the developing retinotectal projection in the zebrafish embryo. *J. Neurosci.* *8*, 4513–4530.
- Stuermer, C.A., Rohrer, B., and Munz, H. (1990). Development of the retinotectal projection in zebrafish embryos under TTX-induced neural-impulse blockade. *J. Neurosci.* *10*, 3615–3626.
- Takamori, S., Rhee, J.S., Rosenmund, C., and Jahn, R. (2001). Identification of differentiation-associated brain-specific phosphate transporter as a second vesicular glutamate transporter (VGLUT2). *J. Neurosci.* *21*, RC182.
- Tokuoka, H., Yoshida, T., Matsuda, N., and Mishina, M. (2002). Regulation by glycogen synthase kinase-3beta of the arborization field and maturation of retinotectal projection in zebrafish. *J. Neurosci.* *22*, 10324–10332.
- Trowe, T., Klostermann, S., Baier, H., Granato, M., Crawford, A.D., Grunewald, B., Hoffmann, H., Karlstrom, R.O., Meyer, S.U., Muller, B., et al. (1996). Mutations disrupting the ordering and topographic mapping of axons in the retinotectal projection of the zebrafish, *Danio rerio*. *Development* *123*, 439–450.
- Tsodyks, M.V., and Markram, H. (1997). The neural code between neocortical pyramidal neurons depends on neurotransmitter release probability. *Proc. Natl. Acad. Sci. USA* *94*, 719–723.
- Wässle, H., and Boycott, B.B. (1991). Functional architecture of the mammalian retina. *Physiol. Rev.* *71*, 447–480.
- Watkins, J.C., Pook, P.C., Sunter, D.C., Davies, J., and Honore, T. (1990). Experiments with kainate and quisqualate agonists and antagonists in relation to the sub-classification of 'non-NMDA' receptors. *Adv. Exp. Med. Biol.* *268*, 49–55.
- Williams, D.R., and Coletta, N.J. (1987). Cone spacing and the visual resolution limit. *J. Opt. Soc. Am. A* *4*, 1514–1523.
- Wojcik, S.M., Rhee, J.S., Herzog, E., Sigler, A., Jahn, R., Takamori, S., Brose, N., and Rosenmund, C. (2004). An essential role for vesicular glutamate transporter 1 (VGLUT1) in postnatal development and control of quantal size. *Proc. Natl. Acad. Sci. USA* *101*, 7158–7163.
- Zhang, L.I., Tao, H.W., Holt, C.E., Harris, W.A., and Poo, M. (1998). A critical window for cooperation and competition among developing retinotectal synapses. *Nature* *395*, 37–44.
- Zucker, R.S., and Regehr, W.G. (2002). Short-term synaptic plasticity. *Annu. Rev. Physiol.* *64*, 355–405.